Co-funded by the Walloon region

Landfill characterization : the landfill of Onoz (Wallonia, Belgium)

Date: January, 2020

SUBJECT:	The landfill of Onoz -						
☒	report	☐	information	☐	consideration	☐	decision
To:	…			From:	ULiege and BGS		

The landfill of Onoz (Wallonia, Belgium)

SITE DESCRIPTION

History

The site which has a total surface area of 6 ha lies in a former quarry in the village of Onoz (province of Namur, Walloon Region, Belgium) where limestone was extracted from 1902 to 1967 and lime produced from 1932 to 1967 (see Fig.1A). At the end of quarrying activities, the eastern pit was first progressively filled with slaked lime (1967-1971, see Fig. 1B) and then with fly ash (1971-1976, see Fig. 1C). From 1977 to 1988, the central and lower parts of the site were used as a landfill where various types of waste materials including inert, household, toxic and dangerous industrial waste were deposited. As illustrated in the aerial photograph of 2018 (Fig. 1D), nowadays vegetation covers a large part of the site and the evidences of the presence of lime and fly ash is difficult to infer visually.

Geology and hydrogeology

The local geology consists in Carboniferous stratified limestone containing dolomite beds from the Onoz and Lives Formations (Delcambre & Pingot, 2008). According to available hydrogeological data, the piezometric level is close to the bottom of the quarry at an altitude of approximately 105 m. Groundwater flow is directed towards the Orneau river which lies at 100 m west of the site (see Fig. 1).

Past studies

Prior to our investigations, two studies had already been conducted on the site to characterize the different deposits (Aenergyes, 2013; Verdi, 1995). In total, 26 trenches were made: 12 in 1993 (Verdi, 1995) and 14 in 2012 (Aenergyes, 2013). Although limited in depth, they still provided information regarding the nature of the geological background, types of waste deposits and contamination levels. However, they did not allow to delineate precisely the lateral and vertical extent of the anthropogenic deposits nor the volumes impacted hence the use of geophysical methods to fill the gap.

Remote sensing data

Beside the aerial photographs taken at different periods which already provide a lot of information regarding the location of lime and fly ash deposits, we can also resort to Laser Detection And Ranging (LIDAR) data which provide high-resolution topography maps to better assess the possible boundaries between different waste deposits (Fig. 1E). Based on historical and LIDAR data, the surface area of the site covered by lime and ash is 12,000 m² (referred to as Zone I, yellow contour in Fig.1E) whereas the heterogeneous waste deposits cover a surface area of 5,000 m² (referred to as Zone II, green contour in Fig.1E).

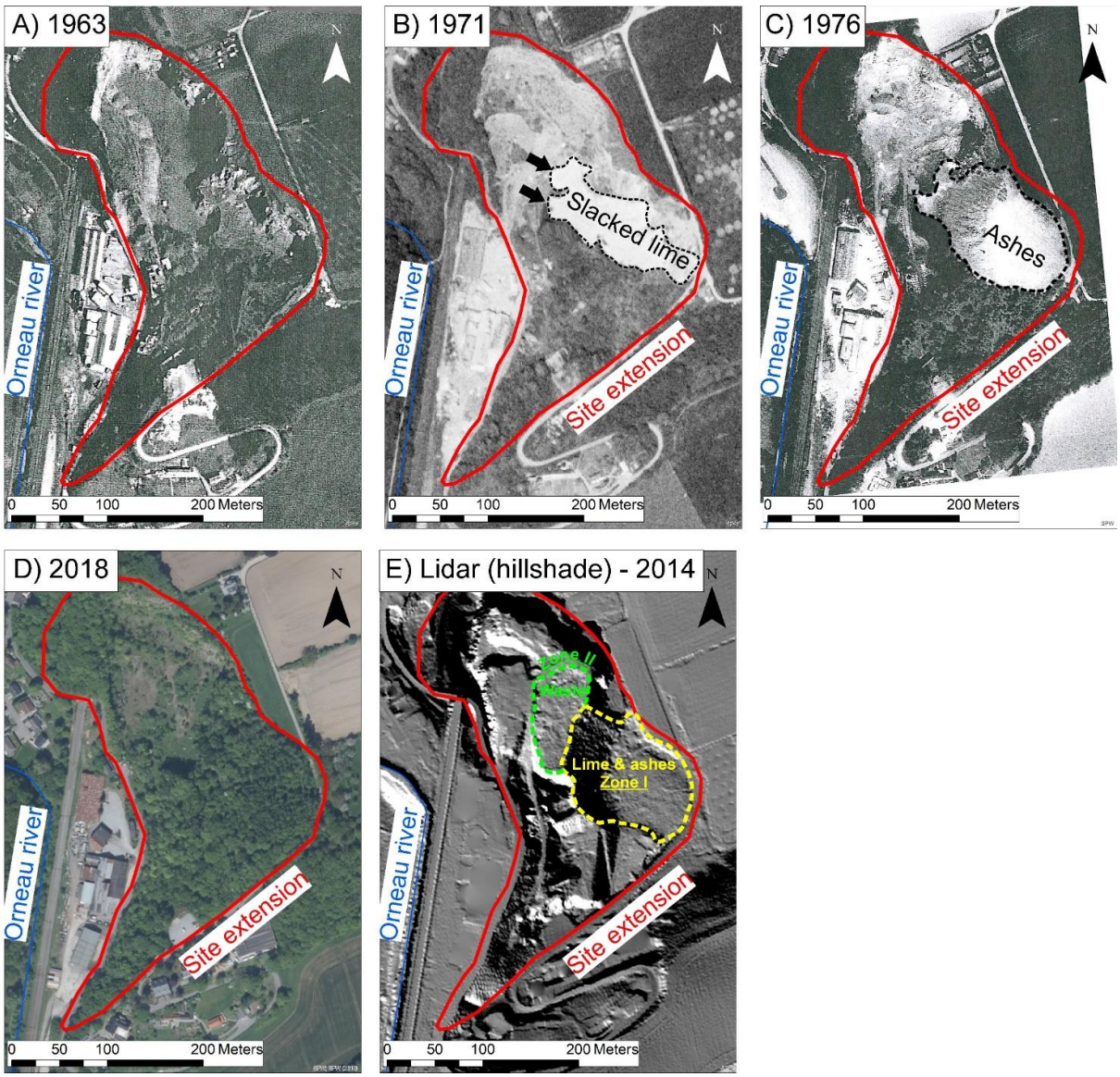

Figure 1: Aerial photographs of the Onoz site in A) 1963, B) 1971, C) 1976 and D) 2018. The hillshade image obtained with LIDAR data is displayed in E. We can observe the progressive filling of the eastern pit (A) with slaked lime (B) and fly ash (C). The aerial photograph of 2018 is more difficult to interpret because of the presence of vegetation (D). The hillshade view of the site obtained with LIDAR data provides more insights allowing the infer possible contours for the anthropogenic deposits (Zone I - fly ash and lime deposits; Zone II – heterogeneous waste deposits). Map background images B, D and E are coming from Service Public de Wallonie (2018) whereas Map background images A and C are taken from Verdi (1995).

EXPERIMENTAL SETUP

Two geophysical surveys were conducted on the landfill site. The first one in 2018 aimed to 1) estimate the lateral extent of the anthropogenic deposits and 2) identify sampling zones. The second geophysical survey, conducted in 2019, aimed to 1) further improve the characterization of the waste materials and 2) provide an estimation of waste volumes that can be used for the development of a resource distribution model (see Deliverable T3.1.1).

Selected geophysical methods

To map physical properties of the landfill, we used two different methods: frequency-domain electromagnetic induction (EM) and magnetometry (MAG). EM probes simultaneously electrical and magnetic properties of the subsoil at one or several depths depending on the device used. MAG measurements consist in measuring the total magnetic field of the earth which is reduced or strengthened in the vicinity of magnetic objects creating magnetic field anomalies. Magnetic measurements can also be carried out in vertical gradient mode which reduces the effect of temporal magnetic variations (Roberts et al., 1990) and allows to identify shallow buried magnetic objects. Both EM and MAG allow to cover large areas in a relatively short time. They were already successfully used to locate boundaries of a landfill (De Iaco et al., 2000; Dumont et al., 2017).
Profiling and imaging methods implemented on the site include Electrical Resistivity Tomography (ERT), Induced polarization (IP), Seismic Refraction Tomography (SRT), Multichannel Analysis of Surface Waves (MASW) and Horizontal to Vertical Spectral Ratio of Noise (HVSRN). Though slower than mapping methods, they provide more in-depth information about the subsoil properties. In this contribution, we will focus on the results obtained with the ERT and IP method which allows to study the spatial distribution of the low-frequency resistive and capacitive characteristics of the soil (Binley & Kemna, 2005).

Instrumentation and acquisition setup

During the first geophysical campaign, we used a conductivity meter model EM31-Mk2 from Geonics. Ground electrical conductivity and in-phase (related to magnetic susceptibility) measurements were recorded simultaneously with an effective exploration depth of about six meters. During the second geophysical survey, a DUALEM-4 with an antenna of 2 m was used and allowed to map the same properties at two other depths levels (0.5 m and 2.3 m). Magnetic data were acquired during the second geophysical survey with a portable caesium magnetometer model G-858 from Geometrics. All data were recorded in vertical gradient mode with 1 m separation between sensors and 0.6 m above ground level. For positioning, both EM and MAG data were continuously synchronized with a GPS system (no RTK). The spatial coverage of the site with both methods is illustrated in Fig 2A. Note that the area not covered in the middle of the image was inaccessible because of the hillslope.
ERT and IP measurements were collected in both geophysical surveys with an ABEM Terrameter LS (12 recording channels, resolution of 3 nV at 1 s integration time). During the first geophysical survey, three profiles were acquired using 64 electrodes spaced by 1.5 m. Two of the profiles included ERT and IP measurements whereas the third one only consisted in ERT measurements. For each profile, we used a dipole-dipole configuration (Dahlin & Zhou, 2004) with a maximum ‘a’ factor limited to 15 m and a ‘n’ factor limited to 8. For the IP measurements, the electrical current was injected for 2 s (with an integration window of 1.7 s for the electrical resistance measurements) and the decay of electrical potential after current shut off was measured for 3 s. For the third profile, the current injection was set to 0.8 s (with an integration window of 0.5 s). Both types of acquisition were repeated at least twice to estimate the repetition error. Location of ERT and IP profiles is presented in Fig. 2B. During the second geophysical survey, four profiles of 32 electrodes spaced by 3 m were setup simultaneously to collect 3D ERT and IP data. For data acquisition, we used the procedure presented in Van Hoorde et al. (2017), i.e. a 2D dipole-dipole configuration for inline measurements (maximum ‘a’= 10 m and ‘n’=6), with cross-lines measurements also using a dipole-dipole configuration . A full dataset of reciprocal measurement was collected after the measurements in normal mode to improve model reliability (LaBrecque et al., 1996). Geometry of the implemented setup is shown in Fig. 2C.

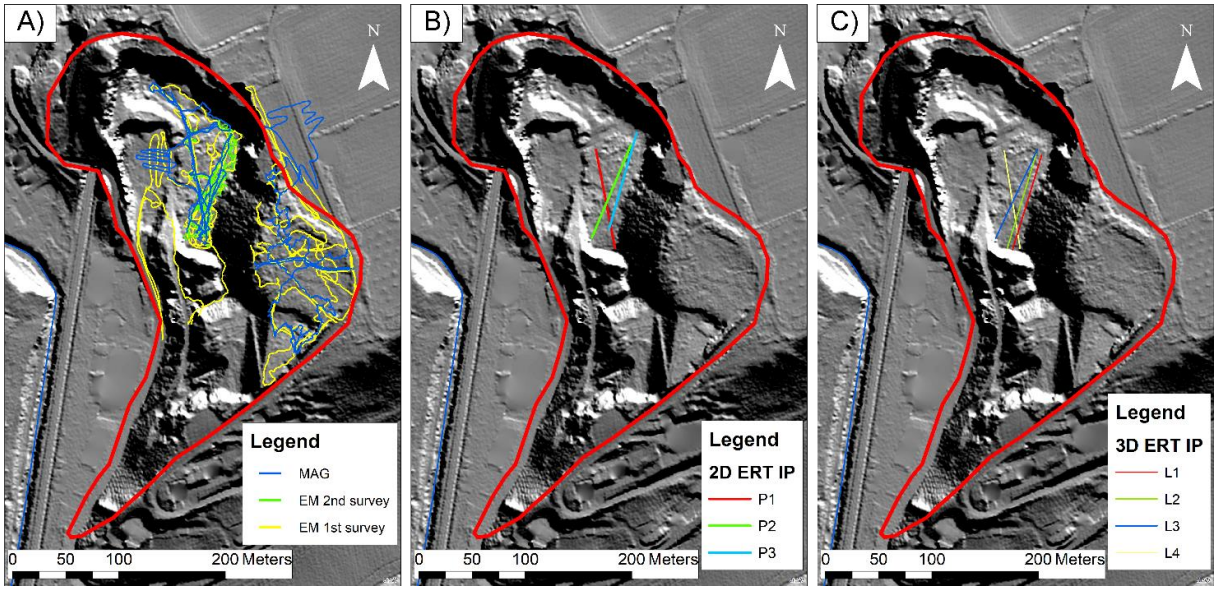

Figure 2: Geophysical coverage of the Onoz site with A) mapping methods (MAG and EM), B) 2D ERT-IP and C) 3D ERT IP.

Data processing

Maps presenting MAG and EMI data were simply obtained by linearly interpolating data collected. For MAG data, we subtracted the earth magnetic field measured outside the landfill from the total magnetic field measured in the landfill in order to highlight the magnetic anomalies due to metallic objects. For ERT and IP, we applied a filter to remove all data characterized by a repetition and reciprocal error (whenever available) larger than 5%. Moreover, IP data exhibiting an inconsistent decay were also discarded from the datasets.

Inversion of electrical data

2D ERT and IP data collected during the first geophysical survey were inverted with Res2Dinv software (Loke & Barker, 1996) using a robust constraint on the data and on the model (Loke et al., 2003). 3D data collected in the second geophysical campaign were inverted with BERT(Günther et al., 2006; Rücker et al., 2006) using individual errors estimated from reciprocal measurements to weight the data. Model obtained with BERT satisfies the error weighted chi-square, $\chi^2 = 1$ meaning that the data were fitted to their error level.

RESULTS AND DISCUSSION

Mapping methods

Figure 3 shows maps of electrical conductivity and in-phase component of the EM data at approximate exploration depths of 6, 2.3 and 0.5 m. Figure 4 shows the results of the MAG survey (total magnetic field and vertical magnetic gradient).

EM results

During the first geophysical survey, only the exploration depth of 6 m was measured. Maps obtained after the interpolation of EM data reveal large variations of electrical properties. Two zones can be

distinguished in both conductivity and in-phase maps (Fig. 3A and B). In Zone I, a very high electrical conductivity anomaly is observed and seems to extent north-westwards down the slope whereas in Zone II, much lower conductivity is observed (Fig. 3A). Similar trend is also visible in the in-phase component image (Fig. 3B).

For visualization purpose, we displayed the areas characterized by electrical conductivities larger than 40 mS/m (i.e. <25 Ohm.m) in blue (Fig. 3A). This threshold was chosen according to the electrical conductivity of a sample of fly ash collected on the site and measured in laboratory. We interpret the highly conductive zone as the lateral extent of ash/lime deposit. Given the high electrical contrast with the surrounding areas (i.e., waste deposits or bedrock), it is easy to draw the contour of this high electrical conductivity zone. Looking at the aerial map of 1971 (Fig. 2B), we notice a white structure (slaked lime) which presents two lobes in its western end (see black arrows in Fig. 2B). The two lobes are also visible in the EM map (Fig. 3A). In the aerial photograph of 1976 (Fig. 2C), i.e. almost at the end of the ash dump, the extent of the zone affected by the spills can easily be delineated (see dashed black contour in Fig. 2C). When reporting this zone in the EM map (Fig. 3A), we observe an almost perfect match with the high conductive area. This confirms the ability of the EM data to discriminate the fly ash/lime materials from the background.

During the second geophysical survey, EM data were only collected in Zone II at two different investigation depths. Due to the field inaccessibility, some areas remained uninvestigated hence the gaps observed in the maps. At 2.3 m depth, two zones with contrasted electrical properties are detected (Fig. 3C). To the south, we still observe high electrical conductivity related to the slope deposits whereas to the north, the electrical conductivity is higher indicating a potential influence of the bedrock. In-phase measurements (related to magnetic susceptibility) at 2.3m (Fig. 3D) exhibit a lot of heterogeneities, particularly in the southern part of the investigated zone indicating a potential higher metallic content. At 0.5 m depth, we distinguish two very conductive zones (likely related to ash and lime materials left on the soil surface after sampling) that are separated by a less conductive zone (inert deposits). In the northern part of the EM map (Fig. 3A, C, E), we observe lower electrical conductivity indicating the limit of the landfill area. In-phase measurements exhibit similar pattern than at 2.3 m depth but with higher amplitude.

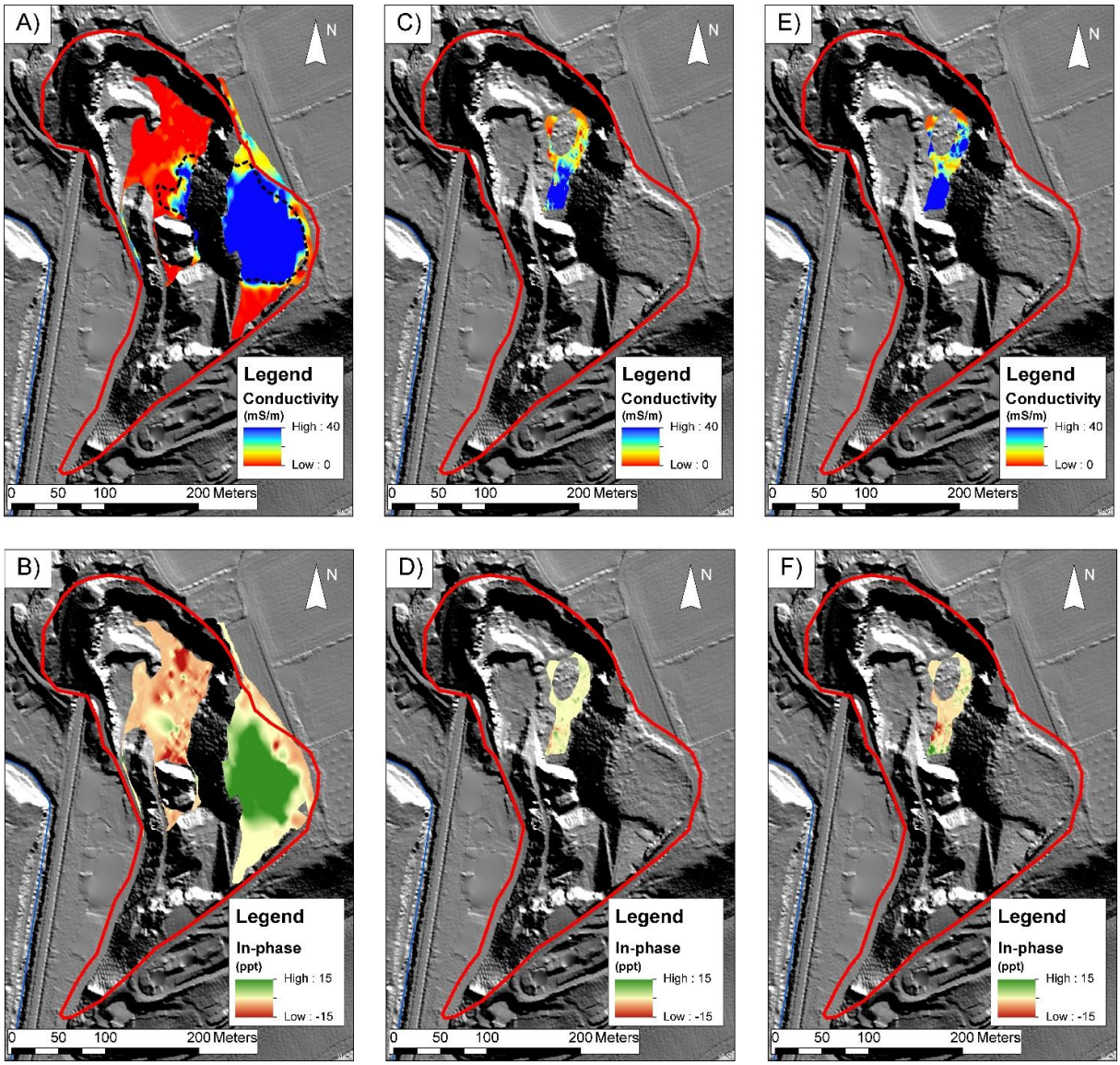

fv*phase maps related to magnetic susceptibility (B, D, F) at a sounding depth of 6 m (A, B), 2.5 m (C, D) and 0.5 m (E,F). Maps A and B allow to delineate the lateral extent of fly ash/lime which fits very well with the contour drawn from the aerial photograph of 1976 (see Fig. 2C).*

MAG mapping

Both total magnetic field and magnetic field gradient show strong anomalies in Zone II indicating the presence of shallow buried magnetic objects (Fig. 4A and B). The method proves really adapted to delineate the extent of the waste deposits which contain buried metallic scraps. Anomalies that are detected in Zone I are simply related to metallic objects (barrels, rebar, etc.) that were visible at the soil surface.

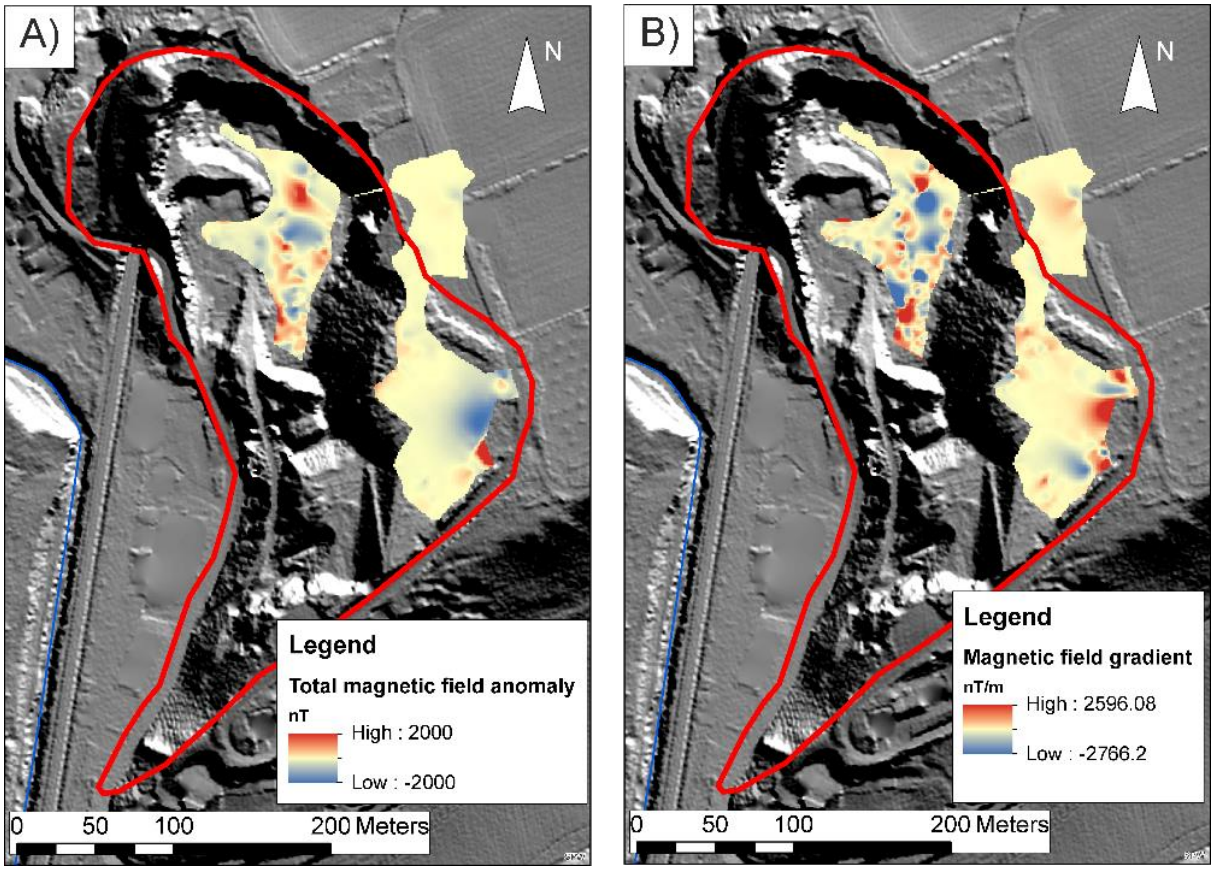

Figure 3: Results of MAG surveys with total magnetic field measured (A) and magnetic field gradient (B). The large anomalies observed in Zone II are attributed to buried magnetic objects (rebars, car parts, etc.).

Imaging methods

Figures 5 and 6 show respectively the inversion results of 2D and 3D ERT/IP data.

2D ERT and IP profiles

Resistivity sections provided in Figures 5A, 5C and 5E exhibit similar patterns. We observe very high resistivity structures (>1000 Ohm.m) at depth, particularly in the northern part of the profiles (from 40 m along P1, 30 m along P2 and 22 m along P3). At the same depth but in the southern part of the profiles, we observe much lower resistivity. The transition between both zones is sharp and vertical. Above these structures, very low electrical resistivity (around 10 Ohm.m) areas are visible at 2 to 3 meters depth. Their lateral extent is limited by more resistive structures suggesting a lens geometry.
P1 and P2 exhibit similar patterns of chargeability (Figures 5B and 5D): spots of very high chargeability are present close to the surface and are underlain in the middle of the profiles by a zone of very low chargeability whereas medium chargeabilities are visible on the edges of the model.
To study model reliability, we computed the depth of investigation index - DOI (Oldenburg & Li, 1999). When selecting a threshold on the computed DOI at 0.1, the resulting depth of investigation is around 12 m meaning that we can still interpret reliably the models to that depth.
The very resistive structure observed in the ERT profiles is characteristic of limestone bedrock (= bottom of the former quarry). Given the very high resistivity, the bedrock is also assumed to be poorly fractured. The horizontal discontinuity observed in all profiles at the level of the bedrock may either reveal a fractured zone containing more water, different lithology (dolomite beds), the presence of leachates (or pollution) or a combination of all these factors. Unfortunately, data available do not allow

to determine which one(s) is (are) responsible of the electrical signature observed. Furthermore, in P1, a vertical shift seems to occur in the bedrock at the distance of 40 m from the beginning of the profile (also observed in P3 at 19 m). Such step in the bedrock is not reported in the historical documents. The very low electrical resistivity anomalies observed above the bedrock in all profiles correspond likely to fly ash/lime material deposits also detected with EM data. Closer to the soil surface, models exhibit more heterogeneity which is consistent with the heterogeneity of the waste materials present in Zone II.

Concerning the chargeability models (Figs. 5B and 5D), the very high chargeabilities observed close to the surface are likely related to metallic scraps that were identified during previous sampling (e.g. car parts). The very low chargeability observed below these hot spots corresponds in the middle of the profiles to the zones where low resistivity was also measured, i.e. the fly ash and lime deposits. In the southern part of the chargeability models, values obtained are slightly higher indicating a potential higher metallic or plastic content.

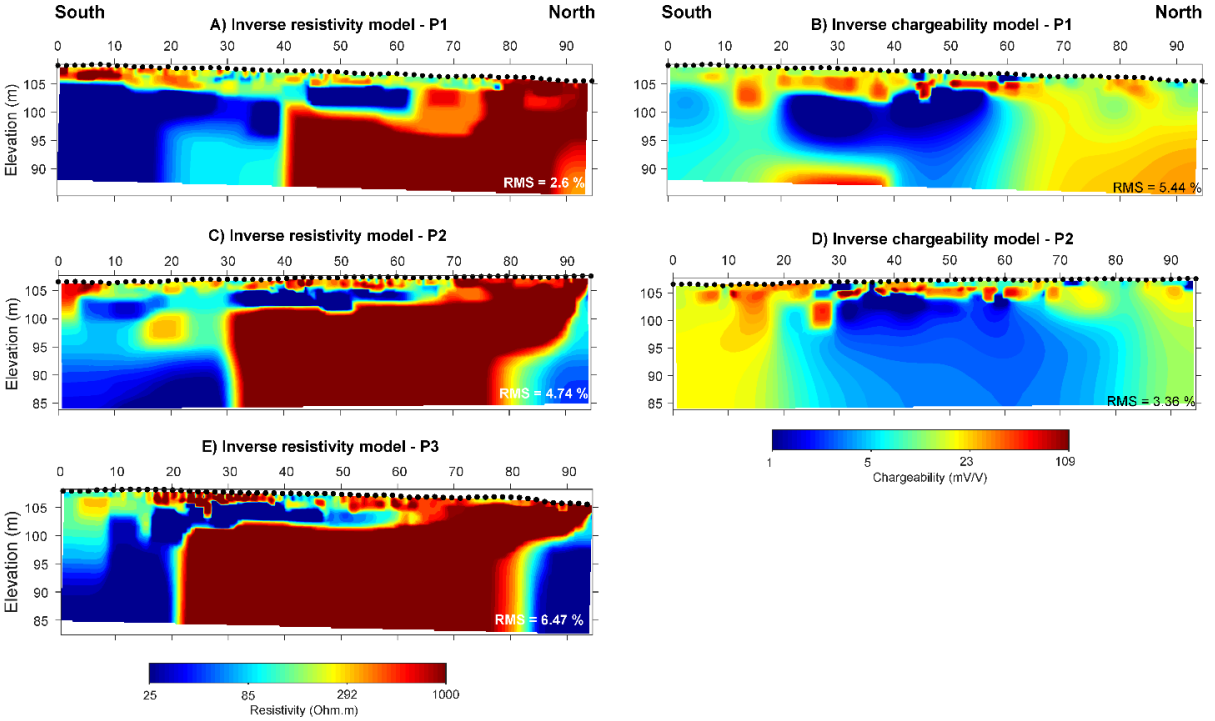

Figure 4: Resistivity (A, C, E) and chargeability (B, D) models obtained inversion of data collected in P1 (A, B), P2 (C, D) and P3 (E). The limestone bedrock is characterized by very high electrical resistivity. Very low resistivity zones are interpreted as fly ash/lime. Waste deposits close to the soil surface are rather characterized by more heterogeneous electrical properties.

3D ERT and IP

3D resistivity model (Fig. 6A) is consistent with the previous results. Even though no electrodes were implemented in the slope between Zones I and II, the model is still able to resolve the low electrical resistivity of fly ash and lime. In the northern part, the bedrock appears as a very resistive structure (>300 Ohm.m). The area marked by a dashed green polygon exhibits more heterogeneity representative of buried waste. Lime and fly ash are characterized again by much lower electrical resistivity. By applying a threshold on electrical resistivity in order to display only the model cells with resistivity lower than 25 Ohm.m, one can try to estimate the volume of fly ash and lime present in Zone II (See Fig. 6B). However, as the 3D model does not allow to detect the bedrock in the southern

part of the investigated area, the estimated volume is still biased. More data are required to further constrain the model and improve its reliability.

3D chargeability model (Fig. 6C) delivers also valuable information regarding landfill composition. In contrast with results provided by Res2dinv, lime and fly ash exhibit high chargeability whereas the bedrock and inert waste is characterized by much lower chargeability. The discrepancy observed between the two models makes their interpretation tricky and should be further investigated with new data.

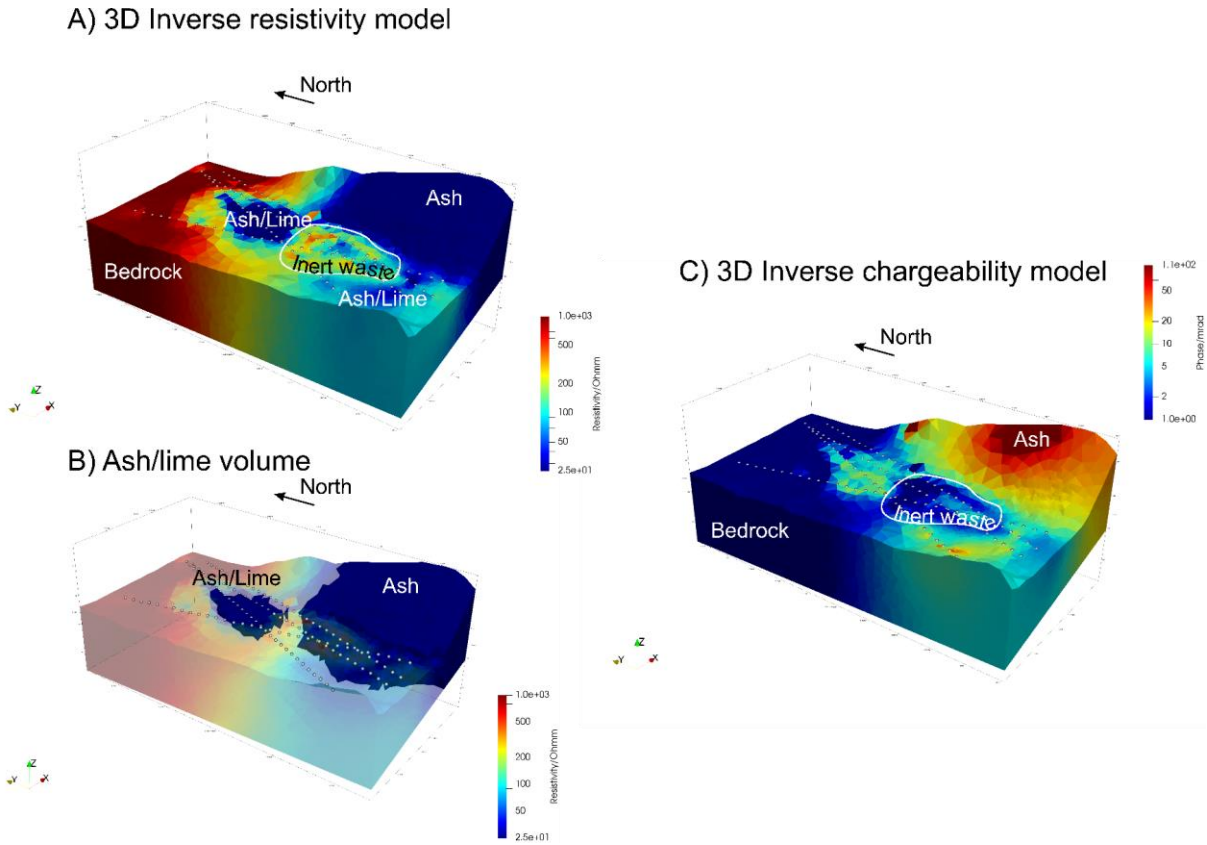

Figure 5: 3D ERT (A) and IP (C) models of Zone II with a proposition of volume of ash/lime estimation by applying a threshold on electrical resistivity value (B).

Sampling results

Based on the results of the first geophysical survey, we proposed a sampling plan which targeted zones where geophysical anomalies were detected or where geophysics alone did not allow to delineate the horizontal/vertical extent of the waste deposits. Sampling was carried out in May and August 2018 and permitted to estimate more accurately the volumes of heterogeneous waste, fly ash and lime deposits present in the landfill as well as to detect the presence of contaminants *(*Irco*, 2018)*. In total, 10 trenches (1 in Zone I, 8 in Zone II and 1 in a non-suspect area) and 5 boreholes (2 in Zone I and 3 in Zone II) were realized. To compare geophysical results with sampling results, we correlate boreholes and trenches information on top of the ERT and IP models (Fig.7). To further compare our results with ground truth data, we also display the trenches that were realized in 1993 and in 2012 . Observations made during the different sampling phases generally validate our interpretation of ERT and IP models. The match between the interpretation of ERT profiles and the trenching data is particularly good in P2 and P3. In P1, the bedrock depth provided by ERT seems to be a little overestimated (see for example

F2, F12 and F19). Still some uncertainties remain concerning the depth of the bedrock in the southern part of the profiles. In that zone, only one borehole (not shown in this report) drilled at 10 m south of P3 detected the bedrock at 4.2 m depth. Based on the correlation between geophysical data and waste samples, fly ash and slaked lime volumes were estimated at 160,000 m^3 and 48,000 m^3, respectively.

Chemical analyses performed on collected samples revealed the presence of several contaminants. These include heavy metals (in heterogenous waste deposits, lime and fly ash), mineral oils (in lime and fly ash), HAP (in heterogenous waste deposits , lime and fly ash), CVOC (inheterogenous waste deposits, lime and fly ash), PCB (in heterogenous waste deposits and lime) and some organochlorides (in lime and fly ash). The presence of all these contaminants may explain the particular geophysical signatures observed in the different deposits. For instance, it has already been reported that old contamination in mineral oils may result in a large decrease of electrical resistivity (e.g. Caterina et al., 2017; Flores Orozco et al., 2012) which may partly explain the very low electrical resistivity observed in lime and fly ash deposits.

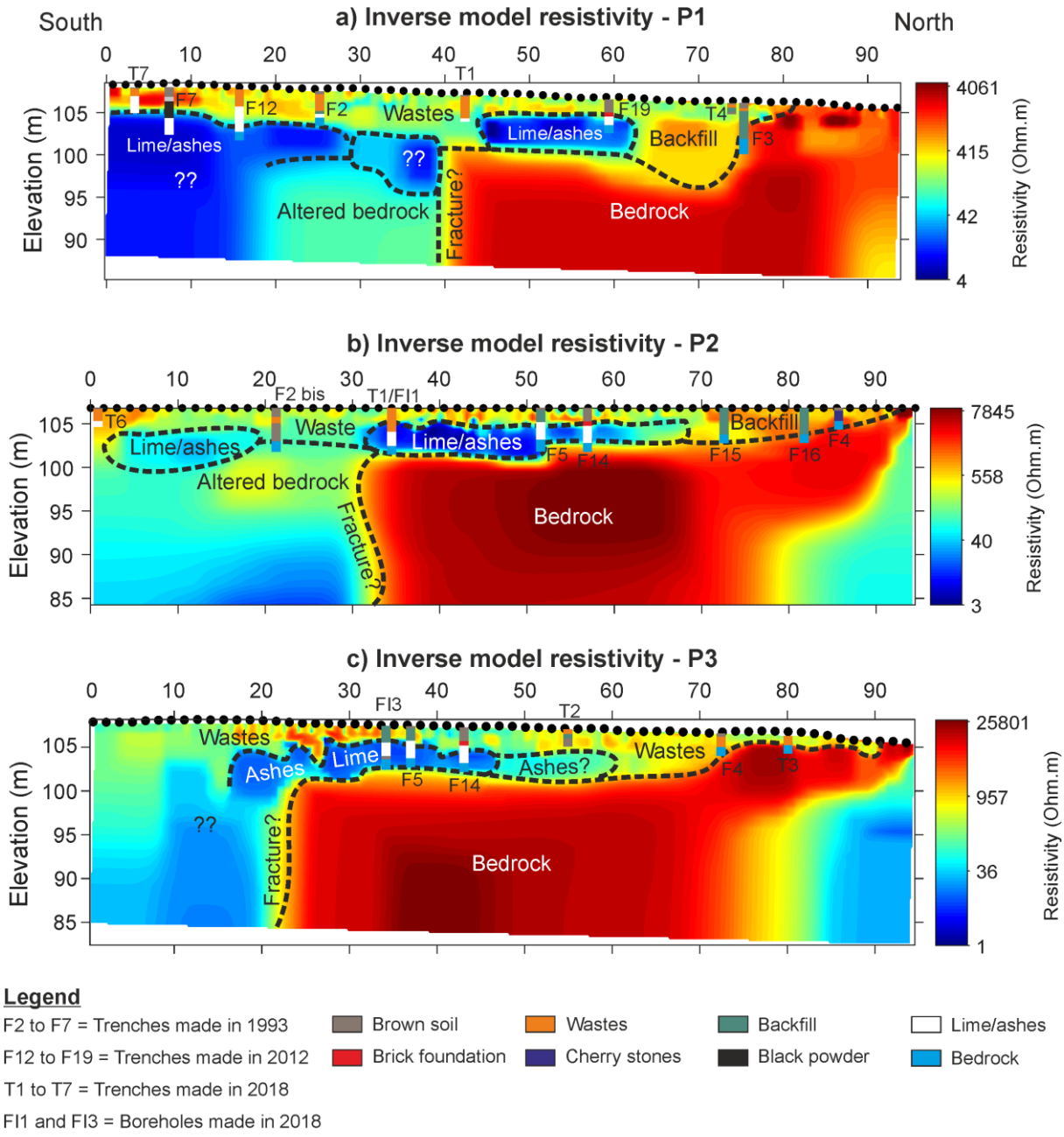

Figure 6: Interpretation of 2D ERT profiles together with borehole/trench data. The comparison of ground truth data with ERT models shows generally a good fit which validates our models.

ESTIMATION OF THE GEOPHYSICAL COSTS

The value for money of geophysical characterization has been estimated based on the number of trenches and boreholes that it allowed to spare compared to a classical characterization only relying on a "drilling-sampling-analysis" scheme. Such scheme was defined in Onoz as:

- 1 borehole of 20 m per 250 m² in the upper part of the landfill
- 1 borehole of 6 m + 1 trench per 250 m² in the lower part of the landfill.

Considering respectively an area of 8,000 m² and 4,000 m² in Zone I and Zone II, the total length of boreholes to be conducted by classical approach should amount to 736 m. In addition, 16 trenches should be conducted. With geophysical data, even though 10 trenches have actually been carried out, only 5 boreholes were conducted for a total length of 65 m. Taking into account the price of the first geophysical survey, we estimated that the use of geophysics and guided sampling allowed to reduce the characterization costs by 75% for this site.

However, geophysics cannot be seen as a silver bullet as it always needs to be validated or calibrated with complementary ground truth data. For example, selected geophysical methods did not allow to clearly discriminate lime from the fly ash, nor to estimate the depth to bedrock in the southern and eastern part of the site. Moreover, geophysics cannot provide analytical data regarding the contamination levels encountered.

CONCLUSIONS

Geophysical exploration proved useful to help characterize the landfill of Onoz. EM mapping method allows to clearly delineate the lateral extent of the ash and lime deposits which are characterized by high electrical conductivity whereas MAG mapping reveals well suited to delineate the extent of the waste in the lower part of the site due to the presence of metallic scraps. ERT and IP imaging provide valuable information regarding the type and (lateral and vertical) extent of the different deposits present in the landfill. Our results allowed to guide the sampling in areas of particular electrical signature or where the uncertainty related to geophysical imaging remained too high. The coupling of geophysical data with guided samples is essential to correctly interpret the data and ensure the reliability of the interpretation.

REFERENCES

Aenergyes. (2013). *Nonet s.a. Réhabilitation du dépotoir de la carrière d'Onoz*.

Binley, A., & Kemna, A. (2005). DC Resistivity and Induced Polarization Methods. In Y. Rubin & S. Hubbard (Eds.), *Hydrogeophysics* (Vol. 50, pp. 129-156): Springer Netherlands.

Caterina, D., Flores-Orozco, A., & Nguyen, F. (2017). Long-term ERT monitoring of biogeochemical changes of an aged hydrocarbon contamination. *Journal of Contaminant Hydrology, 201*, 19-29.

Dahlin, T., & Zhou, B. (2004). A numerical comparison of 2D resistivity imaging with 10 electrode arrays. *Geophysical Prospecting, 52*, 379-398.

De Iaco, R., Green, A., & Horstmeyer, H. (2000). An integrated geophysical study of a landfill and its host sediments. *European Journal of Environmental and Engineering Geophysics, 4*, 223-263.

Delcambre, B., & Pingot, J. (2008). Fleurus–Spy (47/1–2): carte géologique de Wallonie au 1/25 000 et sa notice explicative. *Namur: Service Public de Wallonie, DGARNE, 94*.

Dumont, G., Robert, T., Marck, N., & Nguyen, F. (2017). Assessment of multiple geophysical techniques for the characterization of municipal waste deposit sites. *Journal of Applied Geophysics, 145*, 74-83.

Flores-Orozco, A., Kemna, A., Oberdörster, C., Zschornack, L., Leven, C., Dietrich, P., & Weiss, H. (2012). Delineation of subsurface hydrocarbon contamination at a former hydrogenation plant using spectral induced polarization imaging. *Journal of Contaminant Hydrology, 136–137*(0), 131-144. doi:http://dx.doi.org/10.1016/j.jconhyd.2012.06.001

Günther, T., Rücker, C., & Spitzer, K. (2006). Three-dimensional modelling and inversion of DC resistivity data incorporating topography—II. Inversion. *Geophysical Journal International, 166*(2), 506-517.

Irco. (2018). *Rapport: DSE1801 "Etude de caractérisation avec dispense d'étude d'orientation - Décret sols"*.

LaBrecque, D. J., Miletto, M., Daily, W., Ramirez, A., & Owen, E. (1996). The effects of noise on Occam's inversion of resistivity tomography data. *GEOPHYSICS, 61*(2), 538-548. doi:10.1190/1.1443980

Loke, M. H., Acworth, I., & Dahlin, T. (2003). A comparison of smooth and blocky inversion methods in 2D electrical imaging surveys. *Exploration Geophysics, 34*(3), 182-187. doi:http://dx.doi.org/10.1071/EG03182

Loke, M. H., & Barker, R. D. (1996). Rapid least-squares inversion of apparent resistivity pseudosection using a quasi-Newton method. *Geophysical Prospecting, 44*, 131-152.

Oldenburg, D. W., & Li, Y. (1999). Estimating depth of investigation in dc resistivity and IP surveys. *GEOPHYSICS, 64*(2), 403-416.

Roberts, R., Hinze, W., Leap, D., & Ward, S. (1990). Application of the gravity method to the investigation of a landfill in glaciated midcontinent, USA. *Geotechnical and environmental geophysics, 2*, 253-260.

Rücker, C., Günther, T., & Spitzer, K. (2006). 3-d modeling and inversion of DC resistivity data incorporating topography—Part I: Modeling. *Geophysical Journal International , 166*(2), 495-505.

Service Public de Wallonie (Cartographer). (2018). WalOnMap. Retrieved from

http://geoportail.wallonie.be/walonmap

Van Hoorde, M., Hermans, T., Dumont, G., & Nguyen, F. (2017). 3D electrical resistivity tomography of karstified formations using cross-line measurements. *Engineering geology, 220*, 123-132.

Verdi. (1995). *Audit technique du site du depotoir d'Onoz - Rapport final*.

Contact

Feel free to contact us.

Local contact details:

BELGIUM	ATRASOL	renaud.derijdt@atrasol.eu
	Cleantech Flanders / VITO	alain.ducheyne@vito.be
	OVAM	ewille@ovam.be
	SPAQuE	c.neculau@spaque.be
	Université de Liège	f.nguyen@ulg.ac.be
FRANCE	SAS Les Champs Jouault	champsjouault@gmail.com
GERMANY	BAV	pbv@bavmail.de
THE UK	NERC	jecha@bgs.ac.uk

Coordination office:

BELGIUM	SPAQuE Boulevard Maurice Destenay, 13 4000 Liège	c.neculau@spaque.be